Acta Cryst. (1993). B49, 204–213

Structures of the Nickel Gallosilicate Spinelloids

BY R. HAMMOND AND J. BARBIER

Department of Chemistry, McMaster University, Hamilton, Ontario, Canada L8S 4M1

(*Received* 11 *May* 1992; *accepted* 2 *September* 1992)

Abstract

The structures of four spinelloid phases (spinel plus phases V, I and II), forming at 1 atm pressure in the $NiGa_2O_4$–Ni_2SiO_4 system, have been determined from X-ray data collected from single crystals grown from SiO_2-rich melts in the temperature range 1798–1923 K. The results show that, under conditions of constant pressure, a strong correlation exists between the spinelloid structures, their atomic distributions and their chemical compositions. In particular, the Si contents of the tetrahedral sites are found to be strongly correlated with the amount of tetrahedral corner sharing: 6–12, 24–35 and 65% Si in the $T(1)$, $T(2)$ and $T(3)$ sites with zero, one and two shared corners respectively. Consequently, the spinelloid structures accommodate increasing amounts of Ni_2SiO_4 in the order: spinel (6 mol%), phase V (27 mol%), phase I (33 mol%) and phase II (38 mol%). The crystal chemistry of the nickel gallosilicate spinelloids is discussed in comparison with that of their high-pressure aluminosilicate counterparts.

1. Introduction

The sustained interest in the spinelloid structural family stems from the facts that its members are closely related to the spinel structure type (see, for example, Ma, 1974; Horiuchi, Horioka & Morimito, 1980), that they possibly play a role as intermediates in the high-pressure olivine→spinel transformation (see, for example, Hyde, White, O'Keeffe & Johnson, 1982; Madon & Poirier, 1983; Guyot, Gwanmesia & Liebermann, 1991) and that they belong to the broad class of polytypic compounds (see, for example, Price, 1983; Price, Parker & Yeomans, 1985).

Among the five known spinelloid phases (denoted phases I to V), phase III (also known as the β phase) is the most common and has been reported to form at high pressure in a number of synthetic binary-oxide systems such as MO–SiO_2 (M = Mg, Co, Zn) (Ringwood & Major, 1970; Akimoto & Sato, 1968; Syono, Akimoto & Matsui, 1971) and MnO–GeO_2 (Morimoto, Akimoto, Koto & Tokonami, 1969). Detailed single-crystal structure determinations have been carried out for the phases β-Co_2SiO_4 (Morimoto, Tokonami, Watanabe & Koto, 1974), β-Mn_2GeO_4 (Morimoto, Tokonami, Koto & Nakajima, 1972) and β-Mg_2SiO_4 (Sawamoto & Horiuchi, 1990, and references therein). Furthermore, phase III also occurs naturally in shocked meteorites as the mineral wadsleyite, β-$(Mg,Fe)_2SiO_4$ (Price, Putnis, Agrell & Smith, 1983). Until recently, the other four spinelloid phases had only been observed in the pseudobinary $NiAl_2O_4$(spinel)–Ni_2SiO_4(olivine) system in which all phases I to V were found to exist over specific stability fields in terms of pressure and composition (Ma, 1974; Ma & Tillmanns, 1975; Ma & Sahl, 1975; Ma, Shahl & Tillmanns, 1975; Horioka, Takahashi, Morimoto, Horiuchi, Akaogi & Akimoto, 1981; Horioka, Nishiguchi, Morimoto, Horiuchi, Akaogi & Akimoto, 1981). In particular, phases I and II were the only ones to form at atmospheric pressure (Ma, 1974; Akaogi & Navrotsky, 1984) whereas phases III, IV and V formed at increasingly high pressures with phase V existing above approximately 7 GPa (Akaogi, Akimoto, Horioka, Takahashi & Horiuchi, 1982).

During the course of a search for other systems containing spinelloid phases, new compounds isostructural with phase III were discovered at 1 atm pressure in the MgM_2O_4–Mg_2GeO_4 (M = Ga, Fe) systems (Barbier & Hyde, 1986; Barbier, 1989) and, recently, new spinelloids including phases I, II and V were identified, also at atmospheric pressure, in the $NiGa_2O_4$–Ni_2SiO_4 system (Hammond & Barbier, 1991). Also, a new high-pressure (7 GPa) spinelloid phase V has very recently been characterized in the Fe_3O_4–Fe_2SiO_4 system (Ross, Armbruster & Canil, 1992). The present paper reports the structure determinations by single-crystal X-ray diffraction of the nickel gallosilicate spinelloids (including spinel), providing new insights into the crystal-chemical principles governing the formation and stability of the spinelloid structures.

2. Single-crystal growth

Preliminary experiments (Hammond & Barbier, 1991) had shown that the spinelloid phases of the NiO–Ga_2O_3–SiO_2 system only formed at temperatures above 1673 K and that partial melting occurred

0108-7681/93/020204-10$06.00

at temperatures above approximately 1798 K. Accordingly, single crystals of all four nickel gallosilicate spinelloids (spinel and phases I, II and V) were grown at high temperature, between 1923 and 1798 K by slow cooling (1 or 2 K h^{-1}) of silica-rich NiO–Ga_2O_3–SiO_2 melts.

Single crystals of phase II were obtained from a 10 g sample with a bulk composition of $5NiO.Ga_2O_3.2SiO_2$ plus a 30 wt% excess of SiO_2, melted at 1873 K and cooled to 1798 K. Single crystals of spinel, phase I and phase V were grown from a 10 g melt with a slightly different bulk composition corresponding to $3NiO.Ga_2O_3.SiO_2$ plus a 30 wt% excess of SiO_2. Although the melt composition was identical for these three phases, their crystal growth was found to be critically dependent on the exact temperature interval used, with increasingly higher temperatures being required for the crystallization of phase I, phase V and spinel respectively. More specifically, it was observed that no spinel crystals formed at temperatures below 1846 K, no phase I crystals formed at temperatures above 1823 K, and crystals of phases I and V coexisted in samples cooled to 1798 K. The crystals used in the present work were therefore grown over the temperature ranges 1923–1843 K for spinel, 1848–1823 K for phase V and 1843–1798 K for phase I. Note that all the quoted temperatures are those indicated by the furnace temperature controller (CM furnace with $MoSi_2$ heating elements, equipped with an 818P Eurotherm programmable controller and type B thermocouples) and may therefore differ a little (by perhaps 5–10 K) from the actual sample temperature.

In all cases, the spinelloid single crystals were found embedded in a fine-grained polycrystalline silica-rich matrix from which they could easily be extracted after soaking the samples in hydrofluoric acid at room temperature. All four spinelloid phases yielded dark-green crystals. The crystals of spinel were readily indentified by their truncated octahedral shape whereas the crystals of phases I, II and V could only be distinguished by recording X-ray precession photographs of reciprocal-lattice layers of the type $\{hk0\}$ or $\{0kl\}$ (note that the spinelloid unit cells only differ by their b parameters – see, for example, Akaogi *et al.*, 1982). The close structural relationship existing between the spinelloid phases also resulted in the formation of intergrowths, especially in samples cooled to 1798 K containing both phase I and phase V crystals. Single crystals suitable for data collection, *i.e.* apparently single-phase, were selected on the basis of X-ray precession photographs.

3. Data collection and structure refinements

The four data sets were collected on a Siemens *R3m/V* diffractometer using Ag $K\alpha$ radiation. After an empirical absorption correction of the raw data by means of the ψ-scan technique, the structure refinements were carried out using the *SHELXTL-Plus* software package (Sheldrick, 1990). Details of the crystal data, data-collection procedures and structure refinements for the four spinelloid phases are listed in Tables 1–4.

It should be noted that, since no chemical analyses of the crystals were done, the final compositions were determined by refining the metal site occupancies in each spinelloid structure. Based on previous results for the NiO–Al_2O_3–SiO_2 system (Ma, 1974; Akaogi *et al.*, 1982), the four nickel gallosilicate spinelloids were assumed to have compositions on the pseudobinary $NiGa_2O_4$(spinel)–Ni_2SiO_4(olivine) join.

Table 1. *Structure refinement of nickel gallosilicate spinel*

Crystal data			
Chemical formula	$Ni_{2.12}Ga_{3.76}Si_{0.12}O_8$		
M_r	517.8		
Crystal system	Cubic		
Space group	$Fd\bar{3}m$		
Z	4		
a (Å)	8.2522 (6)		
V (Å^3)	562.0 (3)		
D_x (Mg m^{-3})	6.12		
Radiation	Ag $K\alpha$		
Wavelength (Å)	0.56087		
Absorption coefficient (mm^{-1})	12.97		
No. of reflections for lattice parameters	12		
θ range for lattice parameters (° 2θ)	15.62–30.28		
Temperature (K)	298		
Crystal source	SiO_2-rich oxide melt cooled from 1923 to 1843 K at 2 K h^{-1}		
Colour	Dark green		
Description	Irregular truncated octahedron		
Size (mm)	0.05 × 0.05 × 0.05		
Data collection			
Diffractometer type	Siemens *R3m/V*	Collection method	2θ–θ
Absorption correction	Empirical	T_{min}	0.123
		T_{max}	0.223
No. of reflections measured	2267	θ_{max} (° 2θ)	60
No. of independent reflections	203	R_{int}	0.023
No. of observed reflections	150	Criterion	$F > 6\sigma(F)$
No. of standard reflections	3 every 100	Variation	No decay
h_{min}	0	h_{max}	10
k_{min}	−18	k_{max}	18
l_{min}	−18	l_{max}	18
Refinement			
Treatment of H atoms	Not applicable		
F, F^2 or I	F		
No. of parameters refined	9		
No. of reflections used	150		
Weighting scheme	$w = [\sigma^2(F) + 0.0003F^2]^{-1}$		
Extinction correction	$F^* = F_c[1 + 0.002\chi F_c^2/\sin 2\theta]^{-1/4}$		
Secondary-extinction value	$\chi = 0.0047$ (7)		
Atomic scattering factors	Neutral atoms from *SHELXTL-Plus* package		
R	0.020 (0.032 all data)		
wR	0.022 (0.034 all data)		
S	1.03		
$(\Delta/\sigma)_{max}$	0.001		
$(\Delta\rho)_{min}$ (e Å^{-3})	−2.3		
$(\Delta\rho)_{max}$ (e Å^{-3})	1.2		

Table 2. *Structure refinement of nickel gallosilicate phase* V

Crystal data	
Chemical formula	$Ni_{2.53}Ga_{2.93}Si_{0.53}O_8$
M_r	495.7
Crystal system	Orthorhombic
Space group	*Pmma*
Z	3
a (Å)	5.786 (1)
b (Å)	8.776 (2)
c (Å)	8.230 (2)
V (Å^3)	417.9 (1)
D_x (Mg m^{-3})	5.91
Radiation	Ag $K\alpha$
Wavelength (Å)	0.56087
Absorption coefficient (mm^{-1})	11.78
No. of reflections for lattice parameters	26
θ range for lattice parameters (° 2θ)	14.6–30.5
Temperature (K)	298
Crystal source	SiO_2-rich oxide melt cooled from 1848 to 1823 K at 1 K h^{-1}.
Colour	Dark green
Description	Irregular prism
Size (mm)	0.10 × 0.11 × 0.23

Data collection			
Diffractometer type	Siemens *R3m/V*	Collection method	2θ–θ
Absorption correction	Empirical	T_{min}	0.648
		T_{max}	0.752
No. of reflections measured	1805	θ_{max} (° 2θ)	65
No. of independent reflections	1728	R_{int}	Not applicable
No. of observed reflections	977	Criterion	$F > 6\sigma(F)$
No. of standard reflections	3 every 100	Variation	No decay
h_{min}	0	h_{max}	11
k_{min}	0	k_{max}	16
l_{min}	0	l_{max}	15

Refinement	
Treatment of H atoms	Not applicable
F, F^2 or I	F
No. of parameters refined	72
No. of reflections used	977
Weighting scheme	$w = [\sigma^2(F) + 0.0003F^2]^{-1}$
Extinction correction	$F^* = F_c[1 + 0.002\chi F_c^2/\sin 2\theta]^{-1/4}$
Secondary-extinction value	$\chi = 0.0052$ (3)
Atomic scattering factors	Neutral atoms from *SHELXTL-Plus* package
R	0.043 (0.084 all data)
wR	0.048 (0.059 all data)
S	1.53
$(\Delta/\sigma)_{max}$	0.002
$(\Delta\rho)_{max}$ (e Å^{-3})	−3.8
$(\Delta\rho)_{max}$ (e Å^{-3})	2.9

Table 3. *Structure refinement of nickel gallosilicate phase* I

Crystal data	
Chemical formula	$Ni_{2.65}Ga_{2.70}Si_{0.65}O_8$
M_r	490.1
Crystal system	Orthorhombic
Space group	*Pmma*
Z	4
a (Å)	5.778 (2)
b (Å)	11.723 (1)
c (Å)	8.243 (1)
V (Å^3)	558.3 (2)
D_x (Mg m^{-3})	5.83
Radiation	Ag $K\alpha$
Wavelength (Å)	0.56087
Absorption coefficient (mm^{-1})	11.39
No. of reflections for lattice parameters	23
θ range for lattice parameters (° 2θ)	12.9–45.0
Temperature (K)	298
Crystal source	SiO_2-rich oxide melt cooled from 1848 to 1798 K at 2 K h^{-1}
Colour	Dark green
Description	(010) plate
Size (mm)	0.05 × 0.12 × 0.20

Data collection			
Diffractometer type	Siemens *R3m/V*	Collection method	2θ–θ
Absorption correction	Empirical	T_{min}	0.223
		T_{max}	0.654
No. of reflections measured	2871	θ_{max} (° 2θ)	70
No. of independent reflections	2756	R_{int}	Not applicable
No. of observed reflections	1264	Criterion	$F > 6\sigma(F)$
No. of standard reflections	3 every 100	Variation	No decay
h_{min}	0	h_{max}	11
k_{min}	0	k_{max}	24
l_{min}	0	l_{max}	16

Refinement	
Treatment of H atoms	Not applicable
F, F^2 or I	F
No. of parameters refined	71 (isotropic U values for O atoms)
No. of reflections used	1264
Weighting scheme	$w = [\sigma^2(F) + 0.0003F^2]^{-1}$
Extinction correction	$F^* = F_c[1 + 0.002\chi F_c^2/\sin 2\theta]^{-1/4}$
Secondary-extinction value	$\chi = 0.0017$ (1)
Atomic scattering factors	Neutral atoms from *SHELXTL-Plus* package
R	0.058 (0.122 all data)
wR	0.063 (0.073 all data)
S	1.85
$(\Delta/\sigma)_{max}$	0.001
$(\Delta\rho)_{min}$ (e Å^{-3})	−4.2
$(\Delta\rho)_{max}$ (e Å^{-3})	4.2

Furthermore, by analogy again with the aluminosilicate phases (Ma, Sahl & Tillmanns, 1975; Ma & Tillmanns, 1975; Ma & Sahl, 1975; Horioka, Nishiguchi *et al.*, 1981; Horioka, Takahashi *et al.*, 1981), the tetrahedral and octahedral sites of the spinelloid structures were assumed to have mixed Ga/Si and Ni/Ga occupancies, respectively. Therefore, the refinement of the populations of individual tetrahedral sites in each spinelloid structure could be used to derive unit-cell contents or compositions expressed in molar ratios as $m NiGa_2O_4.n Ni_2SiO_4$. Because of the good contrast in atomic number between Ga and Si atoms, the estimated standard deviations on the refined tetrahedral populations were in the range 0.81–1.0%, corresponding to an error of ±0.02 for the compositions listed in Tables 1–4. After determining the tetrahedral occupancies in the initial stages of the refinement, with R factors typically around 10%, the octahedral Ni/Ga distributions were determined by making use of the relationships between bond length, bond valence and cation valence on individual octaheral sites (Skowron & Brown, 1990). In this way, the sites with the shorter bonds were determined to be Ga rich while those with the longer bonds were determined to be

Table 4. *Structure refinement of nickel gallosilicate phase* II

Crystal data			
Chemical formula	$Ni_{2.75}Ga_{2.5}Si_{0.75}O_8$		
M_r	484.4		
Crystal system	Orthorhombic		
Space group	*Imma*		
Z	6		
a (Å)	5.762 (1)		
b (Å)	17.618 (5)		
c (Å)	8.239 (2)		
V (Å^3)	836.4 (4)		
D_x (Mg m^{-3})	5.78		
Radiation	Ag $K\alpha$		
Wavelength (Å)	0.56087		
Absorption coefficient (mm^{-1})	11.09		
No. of reflections for lattice parameters	20		
θ range for lattice parameters (° 2θ)	14.9–29.9		
Temperature (K)	298		
Crystal source	SiO_2-rich oxide melt cooled from 1848 to 1798 K at 2 K h^{-1}		
Colour	Dark green		
Description	Irregular prism		
Size (mm)	0.11 × 0.15 × 0.32		
Data collection			
Diffractometer type	Siemens *R3m/V*	Collection method	2θ–θ
Absorption correction	Empirical	T_{min}	0.152
		T_{max}	0.444
No. of reflections measured	2135	θ_{max} (° 2θ)	70
No. of independent reflections	2050	R_{int}	Not applicable
No. of observed reflections	1272	Criterion	$F > 6\sigma(F)$
No. of standard reflections	3 every 100	Variation	No decay
h_{min}	0	h_{max}	11
k_{min}	0	k_{max}	36
l_{min}	0	l_{max}	16
Refinement			
Treatment of H atoms	Not applicable		
F, F^2 or I	F		
No. of parameters refined	70		
No. of reflections used	1272		
Weighting scheme	$w = [\sigma^2(F) + 0.0003F^2]^{-1}$		
Extinction correction	$F^* = F_c[1 + 0.002\chi F_c^2/\sin 2\theta]^{-1/4}$		
Secondary-extinction value	$\chi = 0.00140$ (7)		
Atomic scattering factors	Neutral atoms from *SHELXTL-Plus* package		
R	0.046 (0.078 all data)		
wR	0.050 (0.057 all data)		
S	1.66		
$(\Delta/\sigma)_{max}$	0.001		
$(\Delta\rho)_{min}$ (e Å^{-3})	−5.4		
$(\Delta\rho)_{max}$ (e Å^{-3})	3.8		

Ni rich, as expected from the ionic radii values [octahedral Ga—O and Ni—O bond lengths of 2.00 and 2.07 Å respectively; see Shannon (1976)]. The Ni and Ga populations were then scaled to give an overall composition consistent with that determined from the tetrahedral Ga/Si populations.

It is also worth noting that, in spite of earlier electron diffraction data indicating a loss of **a**-glide symmetry in some flux-grown crystals of phases II and V (Hammond & Barbier, 1991), only one or two weak forbidden reflections were present in each of the data sets collected for phases I, II and V. These reflections were simply excluded and the refinements were carried out in the *Pmma* (phases I and V) and *Imma* (phase II) space groups determined earlier for the aluminosilicate spinelloids. The final atomic coordinates, isotropic displacement coefficients and site occupancies are listed in Table 5 for the four spinelloid phases.* Due to a slightly poorer quality of the phase I crystal (perhaps from an undetected small amount of phase V intergrowth?), rather large e.s.d.'s were obtained for the coordinates and temperature factors of the O atoms, which were, therefore, only refined isotropically.

4. Description of the crystal structures

The structures of the four nickel gallosilicate spinelloids determined in the present study are shown in Fig. 1 projected along equivalent directions, *i.e.* [100] for phases I, II and V and [$\bar{1}$10] for spinel. The corresponding bond lengths and bond angles for the MO_6 and TO_4 polyhedra are listed in Tables 6–9 and the bonding in the tetrahedral groups of phases V, I and II is further illustrated in Fig. 2. The four phases are isostructural with their counterparts of the NiO–Al_2O_3–SiO_2 system, with the same structural relations between them as described by previous authors (*e.g.* Hyde *et al.*, 1982; Horiuchi, Akaogi & Sawamoto, 1982; Madon & Poirier, 1983).

The octahedral and tetrahedral site occupancies listed in Table 5 reveal some interesting correlations among the spinelloid structures that have not been explicitly established in the case of the aluminosilicate phases, partly because of the difficulty in distinguishing Al from Si by X-ray diffraction. The most obvious correlation concerns the Ga/Si distribution on the tetrahedral sites: the sites labelled $T(1)$ (or simply T in spinel), $T(2)$ and $T(3)$, corresponding to equivalent sites in terms of the number of corners being shared with adjacent tetrahedra (*i.e.* zero, one and two respectively), have similar bond lengths (see Tables 6–9) and similar populations with Si contents increasing from the $T(1)$ to the $T(3)$ sites (see Table 10). It follows from this trend that the spinelloid phases accommodate more and more silicon in their crystal structures when passing from spinel to phases V, I and II. Consequently, their overall compositions become richer in Ni_2SiO_4, *viz.* 6.0, 27.3, 32.7 and 38.0 mol% Ni_2SiO_4 respectively (*cf.* crystal data in Tables 1–4 and Table 10). (Note that, because the crystals were grown from SiO_2-rich melts, these compositions may be regarded as upper limits for the

* Tables of anisotropic displacement coefficients and observed (F_o) and calculated (F_c) structure factors for the nickel gallosilicate spinelloids have been deposited with the British Library Document Supply Centre as Supplementary Publication No. SUP 55542 (19 pp.). Copies may be obtained through The Technical Editor, International Union of Crystallography, 5 Abbey Square, Chester CH1 2HU, England.

Table 5. *Atomic coordinates* ($\times 10^4$) *and equivalent isotropic displacement coefficients* ($Å^2 \times 10^4$)

The octahedral (*M*) and tetrahedral (*T*) sites are occupied by mixtures of (Ni + Ga) and (Ga + Si) atoms respectively.

		x	*y*	*z*	*U**	Population (%Ga)†
Spinel	*M*	5000	5000	5000	59 (1)	47
	T	1250	1250	1250	52 (1)	94 (1)
	O	2555 (1)	2555 (1)	2555 (1)	79 (1)	
Phase V	*M*(1)	7500	1660 (2)	2509 (1)	60 (2)	49
	M(2)	0	0	0	74 (3)	36
	M(3)	5000	3343 (1)	5000	56 (2)	29
	M(4)	7500	5000	2259 (2)	59 (3)	28
	T(1)	2500	0	3769 (2)	59 (3)	88 (1)
	T(2)	2500	3246 (1)	1294 (1)	51 (2)	65 (1)
	O(1)	5079 (17)	0	2465 (5)	78 (16)	
	O(2)	2500	1636 (10)	−15 (7)	135 (14)	
	O(3)	2500	1738 (7)	5049 (6)	92 (13)	
	O(4)	5068 (12)	3310 (6)	2517 (4)	110 (12)	
	O(5)	2500	5000	172 (10)	113 (20)	
	O(6)	2500	5000	5244 (8)	72 (17)	
Phase I	*M*(1)	2500	3756 (4)	2484 (1)	66 (3)	64
	M(2)	0	5000	5000	80 (4)	37
	M(3)	0	2481 (1)	0	64 (3)	30
	M(4)	2500	1245 (3)	2727 (2)	63 (3)	14
	M(5)	0	0	0	58 (4)	14
	T(1)	2500	5000	8780 (2)	61 (3)	90 (1)
	T(2)	2500	2575 (1)	6299 (2)	60 (3)	72 (1)
	T(3)	2500	0	6356 (4)	60 (6)	35 (1)
	O(1)	2500	1233 (10)	243 (9)	106 (12)	
	O(2)	2500	3694 (9)	55 (10)	93 (13)	
	O(3)	2500	1200 (10)	5228 (10)	134 (14)	
	O(4)	2500	3774 (10)	4933 (10)	120 (13)	
	O(5)	−101 (33)	0	2503 (10)	113 (36)	
	O(6)	83 (42)	5000	2531 (10)	107 (38)	
	O(7)	−108 (30)	2523 (5)	7528 (7)	69 (27)	
Phase II	*M*(1)	0	0	0	45 (2)	74
	M(2)	2500	2500	7500	38 (2)	20
	M(3)	2500	851 (1)	7500	44 (1)	26
	M(4)	0	1668 (1)	221 (1)	42 (1)	21
	T(2)	0	4215 (1)	3786 (1)	39 (1)	76 (1)
	T(3)	0	2500	3847 (2)	36 (3)	34 (1)
	O(1)	0	8318 (3)	2269 (5)	71 (8)	
	O(2)	0	−30 (3)	2450 (5)	103 (11)	
	O(3)	0	1694 (3)	2704 (5)	106 (9)	
	O(4)	2515 (10)	2500	16 (5)	75 (11)	
	O(5)	2412 (6)	819 (2)	−20 (4)	78 (6)	

* Equivalent isotropic *U* defined as one third of the trace of the orthogonalized U_{ij} tensor.

† Only the tetrahedral populations have been refined (see text).

Ni_2SiO_4 contents of the nickel gallosilicate spinelloids at 1 atm pressure.) A clear correlation therefore exists between the type of spinelloid phase formed along the $NiGa_2O_4$(spinel)–Ni_2SiO_4(olivine) join and its chemical composition: using the sequence of *T* and *S* boundaries to characterize the individual spinelloid structures [after Hyde *et al.* (1982) – see Fig. 1], phase V (TS^2) is the most spinel-like of the spinelloids and the richest in $NiGa_2O_4$, whereas phase II (TS^2TS^2) is the least spinel-like and the richest in Ni_2SiO_4. This result differs markedly from the pressure *vs* composition phase diagram previously determined for the $NiAl_2O_4$–Ni_2SiO_4 system (Akaogi *et al.*, 1982) in which phase I was reported to be the most $NiAl_2O_4$-rich phase and phase V was found to be richer in Ni_2SiO_4. This difference between the two systems may reflect the influence of pressure on the crystal chemistry of the spinelloid phases (see §5).

The correlation among the octahedral-site occupancies of the nickel gallosilicate spinelloids is less pronounced than for the tetrahedral sites, perhaps as a result of a smaller tendency for the Ni and Ga atoms to order. Nevertheless, in all three phases V, I and II, the *M*(1) sites systematically have the highest Ga content while the *M*(4) sites [plus the *M*(5) site of phase I and the *M*(2) site of phase II] all have a high Ni content. Therefore, the correlation observed between the spinelloid structure type and the chemical composition also extends to the details of the entire atomic distribution with a concentration of Ga atoms in the spinel parts of the structures (around the *S* boundaries) and a concentration of Ni and Si atoms in the nonspinel parts (around the *T* boundaries) (see Table 5 and Fig. 1). Interestingly, a similar distribution is also observed in the structure of the new spinelloid phase V, $Fe_{5.36}Si_{0.64}O_8$, of the Fe_3O_4–Fe_2SiO_4 system with a concentration of

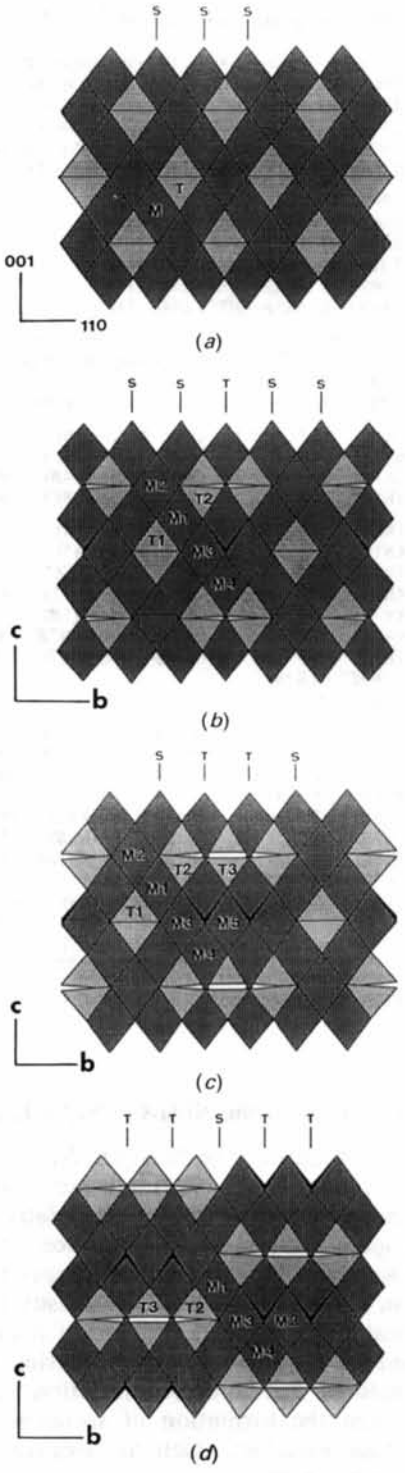

Fig. 1. Equivalent projections of (*a*) nickel gallosilicate spinel, (*b*) phase V, (*c*) phase I and (*d*) phase II. The structures are based on cubic close-packed O atoms with (Ni,Ga) and (Ga,Si) atoms occupying the octahedral (*M*) and tetrahedral (*T*) sites, respectively. The spinelloid structures contain pseudo-antiphase (*S*) and pseudo-twin (*T*) planar boundaries, the latter generating corner-sharing TO_4 tetrahedra. Note the volume reduction of the Si-rich *T*(3) sites in phases I and II.

divalent Fe atoms on the *M*(4) site and of Si atoms on the *T*(2) site (Ross *et al.*, 1992).

The introduction of *T* boundaries and the concentration of silicon in the *T*(2) and *T*(3) sites of the structures lead to distortions of the O-atom packings, increasing in the order phase V, I and II: for instance, the *c*/*a* and *b*/*c* axial ratios deviate more and more from their ideal values (for perfect cubic close packing) with differences of 0.6, 0.9, 1.1 and 0.5, 0.6, 0.8%, respectively. As seen in Figs. 1 and 2, the distortions are most obvious at the *T* boundaries and, in particular, involve displacements of the O atoms located in these planes. Some of these atoms [O(5) in phase V and O(3) in phases I and II] are

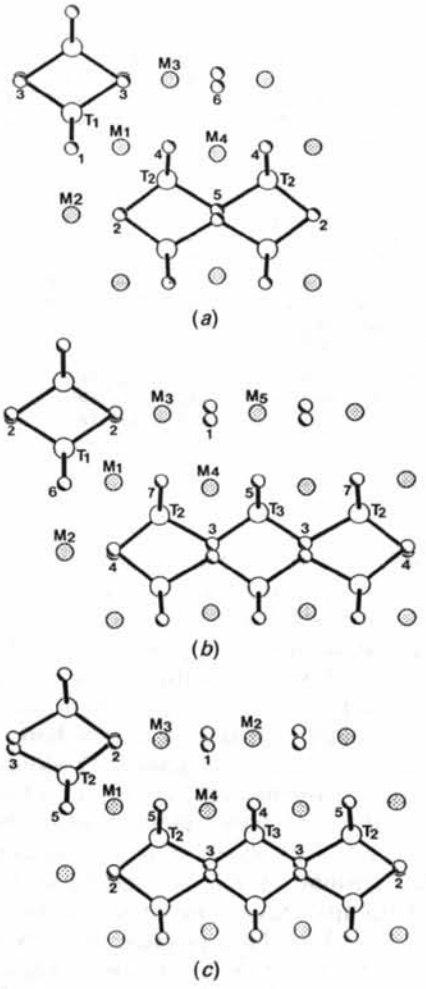

Fig. 2. Details of the bonding within the tetrahedral groups of (*a*) phase V (with TO_4 and T_2O_7 groups), (*b*) phase I (with TO_4 and T_3O_{10} groups) and (*c*) phase II (with T_3O_{10} groups only). Large and small circles represent the metal and O atoms respectively. The numbers near the O atoms correspond to the atom numbers in Tables 5–9. Note the distortions associated with the *T* boundaries and the displacements of the three- and five-coordinated O atoms.

Table 6. *Bond lengths* (Å) *and angles* (°) *in spinel*

M—O	2.019 (1)		
T—O	1.866 (2)		
O—*M*—O	87.4 (1) × 6	O—*T*—O	109.5 × 6
O—*M*—O	92.6 (1) × 6		

Table 7. *Bond lengths* (Å) *and angles* (°) *in phase* V

M(1)—O(1)	2.021 (7)	*M*(2)—O(2)	2.038 (6)	*M*(3)—O(3)	2.020 (4)
M(1)—O(4)	2.019 (6)	*M*(2)—O(1*B*)	2.029 (5)	*M*(3)—O(4)	2.044 (3)
M(1)—O(1*A*)	2.021 (7)	*M*(2)—O(1*C*)	2.029 (5)	*M*(3)—O(6)	2.061 (1)
M(1)—O(2*C*)	2.053 (6)	*M*(2)—O(2*A*)	2.038 (6)	*M*(3)—O(3*B*)	2.020 (4)
M(1)—O(3*B*)	2.010 (5)	*M*(2)—O(2*B*)	2.038 (6)	*M*(3)—O(4*B*)	2.044 (3)
M(1)—O(4*D*)	2.019 (6)	*M*(2)—O(2*D*)	2.038 (6)	*M*(3)—O(6*A*)	2.061 (1)
M(4)—O(4)	2.056 (6)	*T*(1)—O(1)	1.838 (8)	*T*(2)—O(2)	1.776 (8)
M(4)—O(4*A*)	2.056 (6)	*T*(1)—O(3)	1.854 (6)	*T*(2)—O(4)	1.796 (6)
M(4)—O(4*C*)	2.056 (6)	*T*(1)—O(1*B*)	1.838 (8)	*T*(2)—O(5)	1.796 (4)
M(4)—O(4*D*)	2.056 (6)	*T*(1)—O(3*A*)	1.854 (6)	*T*(2)—O(4*E*)	1.796 (6)
M(4)—O(5*A*)	2.000 (8)				
M(4)—O(6*A*)	2.055 (7)				

O(1)—*M*(1)—O(4)	91.9 (3) × 2	O(2)—*M*(2)—O(1*B*)	91.3 (3) × 4
O(1)—*M*(1)—O(1*A*)	87.7 (4)	O(2)—*M*(2)—O(1*C*)	88.7 (3) × 4
O(1)—*M*(1)—O(2*C*)	88.6 (2) × 2	O(2)—*M*(2)—O(2*B*)	89.6 (3) × 2
O(4)—*M*(1)—O(2*C*)	90.6 (2) × 2	O(2)—*M*(2)—O(2*D*)	90.4 (3) × 2
O(1)—*M*(1)—O(3*B*)	92.4 (2) × 2		
O(4)—*M*(1)—O(3*B*)	88.4 (2) × 2		
O(4)—*M*(1)—O(4*D*)	88.4 (2)		
O(3)—*M*(3)—O(4)	91.4 (2) × 2	O(4)—*M*(4)—O(4*C*)	92.4 (3)
O(3)—*M*(3)—O(6)	89.3 (1) × 2	O(4*A*)—*M*(4)—O(4*C*)	86.4 (3) × 2
O(4)—*M*(3)—O(6)	97.0 (3) × 2	O(4*A*)—*M*(4)—O(4*D*)	92.4 (3)
O(3)—*M*(3)—O(3*B*)	91.5 (3)	O(4)—*M*(4)—O(5*A*)	95.9 (1) × 4
O(4)—*M*(3)—O(3*B*)	87.5 (2) × 2	O(4)—*M*(4)—O(6*A*)	84.1 (1) × 4
O(6)—*M*(3)—O(4*B*)	84.2 (3) × 2		
O(6)—*M*(3)—O(6*A*)	90.2 (1)		
O(1)—*T*(1)—O(3)	109.4 (1) × 4	O(2)—*T*(2)—O(4)	111.4 (2) × 2
O(1)—*T*(1)—O(1*B*)	108.6 (4)	O(2)—*T*(2)—O(5)	111.7 (3) × 2
O(3)—*T*(1)—O(3*A*)	110.7 (3)	O(4)—*T*(2)—O(5)	105.2 (2) × 2

Symmetry codes: *A*, $\frac{1}{2}-x, -y, z$; *B*, $-x, y, -z$; *C*, $x, -y, z$; *D*, $\frac{1}{2}-x, y, z$; *E*, $\frac{1}{2}+x, y, z$.

three-coordinated only, being shared by one *M*(4) site and two *T* sites, while the others [O(6) in phase V and O(1) in phases I and II] are five-coordinated, shared by five *M* sites. It appears that the higher Si content of the *T*(3) sites (with two shared corners) relative to that of the *T*(2) sites (with one shared corner) is required to maintain proper bond valence sums around the three-coordinated O atoms. These valence sums are further adjusted by variations in the *T*—O and *M*(4)—O bond lengths (see Tables 6–9) and their values [calculated from the parameters of Brown & Altermatt (1985) and taking into account the mixed occupancies of the sites] are indeed close to ideal, *viz.* 1.95 for O(5) in phase V, 1.98 for O(3) in phase I and 1.97 for O(3) in phase II. On the other hand, the bond valence sums around the five-coordinated O atoms are slightly lower than expected with values of 1.78 for O(6) in phase V, 1.76 for O(1) phase I and 1.78 for O(1) in phase II. This difference, however, may simply be a result of small errors in the distributions of the octahedral Ni and Ga atoms, which have only been determined indirectly (see §3).

Table 8. *Bond lengths* (Å) *and angles* (°) *in phase* I

M(5)—O(1)	2.053 (8)	*M*(2)—O(4)	2.039 (9)	*M*(3)—O(1)	2.066 (8)
M(5)—O(5)	2.064 (8)	*M*(2)—O(6)	2.036 (8)	*M*(3)—O(2)	2.028 (7)
M(5)—O(1*A*)	2.053 (8)	*M*(2)—O(4*A*)	2.039 (9)	*M*(3)—O(1*C*)	2.066 (8)
M(5)—O(1*B*)	2.053 (8)	*M*(2)—O(4*B*)	2.039 (9)	*M*(3)—O(2*C*)	2.028 (7)
M(5)—O(1*C*)	2.053 (8)	*M*(2)—O(4*C*)	2.039 (9)	*M*(3)—O(7*A*)	2.039 (5)
M(5)—O(5*A*)	2.064 (8)	*M*(2)—O(6*A*)	2.036 (8)	*M*(3)—O(7*C*)	2.039 (5)
M(4)—O(1)	2.048 (8)	*M*(1)—O(2)	2.003 (8)		
M(4)—O(3)	2.062 (8)	*M*(1)—O(4)	2.019 (8)		
M(4)—O(5)	2.104 (14)	*M*(1)—O(6)	2.019 (17)		
M(4)—O(5*C*)	2.104 (14)	*M*(1)—O(6*B*)	2.019 (17)		
M(4)—O(7*B*)	2.049 (13)	*M*(1)—O(7*B*)	2.000 (13)		
M(4)—O(7*C*)	2.049 (13)	*M*(1)—O(7*C*)	2.000 (13)		
T(1)—O(2*A*)	1.857 (10)	*T*(3)—O(3)	1.686 (11)	*T*(2)—O(3)	1.838 (11)
T(1)—O(2*B*)	1.857 (10)	*T*(3)—O(3*A*)	1.686 (11)	*T*(2)—O(4)	1.801 (11)
T(1)—O(6*A*)	1.842 (20)	*T*(3)—O(5*B*)	1.675 (16)	*T*(2)—O(7)	1.817 (15)
T(1)—O(6*C*)	1.842 (20)	*T*(3)—O(5*D*)	1.675 (16)	*T*(2)—O(7*D*)	1.817 (15)

O(1)—*M*(5)—O(5)	85.6 (4) × 4	O(4)—*M*(2)—O(6)	87.5 (5) × 4
O(5)—*M*(5)—O(1*A*)	94.4 (4) × 4	O(6)—*M*(2)—O(4*A*)	92.5 (5) × 4
O(1)—*M*(5)—O(1*B*)	89.5 (4) × 2	O(4)—*M*(2)—O(4*B*)	89.7 (5) × 2
O(1)—*M*(5)—O(1*C*)	90.5 (4) × 2	O(4)—*M*(2)—O(4*C*)	90.3 (5) × 2
O(1)—*M*(3)—O(2)	89.8 (3) × 2	O(1)—*M*(4)—O(5)	84.7 (3) × 2
O(1)—*M*(3)—O(1*C*)	89.8 (4)	O(3)—*M*(4)—O(5)	94.0 (3) × 2
O(2)—*M*(3)—O(2*C*)	90.9 (4)	O(5)—*M*(4)—O(5*C*)	91.2 (7)
O(1)—*M*(3)—O(7*A*)	97.8 (4) × 2	O(1)—*M*(4)—O(7*B*)	84.4 (3) × 2
O(2)—*M*(3)—O(7*A*)	91.6 (4) × 2	O(3)—*M*(4)—O(7*B*)	97.0 (3) × 2
O(1)—*M*(3)—O(7*C*)	84.2 (4)	O(5*C*)—*M*(4)—O(7*B*)	90.9 (5) × 2
O(2)—*M*(3)—O(7*C*)	86.5 (4)	O(7*B*)—*M*(4)—O(7*C*)	84.8 (8)
O(1*C*)—*M*(3)—O(7*C*)	97.8 (4)		
O(2*C*)—*M*(3)—O(7*C*)	91.6 (4)		
O(2)—*M*(1)—O(6)	92.6 (3) × 2	O(2*A*)—*T*(1)—O(2*B*)	111.0 (6)
O(4)—*M*(1)—O(6)	88.5 (4) × 2	O(2*A*)—*T*(1)—O(6*A*)	109.4 (3) × 4
O(2)—*M*(1)—O(6*B*)	92.6 (3)	O(6*A*)—*T*(1)—O(6*C*)	108.2 (10)
O(4)—*M*(1)—O(6*B*)	88.5 (4)		
O(6)—*M*(1)—O(6*B*)	87.5 (10)	O(3)—*T*(3)—O(3*A*)	113.0 (7)
O(2)—*M*(1)—O(7*B*)	88.2 (3) × 2	O(3)—*T*(3)—O(5*B*)	108.1 (3) × 4
O(4)—*M*(1)—O(7*B*)	90.7 (3)	O(5*B*)—*T*(3)—O(5*D*)	111.6 (9)
O(6)—*M*(1)—O(7*C*)	92.5 (6)		
O(7*B*)—*M*(1)—O(7*C*)	87.4 (8)	O(3)—*T*(2)—O(4)	112.6 (4)
		O(3)—*T*(2)—O(7)	103.8 (3) × 2
		O(4)—*T*(2)—O(7)	112.0 (3) × 2
		O(7)—*T*(2)—O(7*D*)	112.1 (7)

Symmetry codes: *A*, $x, y, z-1$; *B*, $\frac{1}{2}+x, y, -z$; *C*, $-x, y, -z$; *D*, $\frac{1}{2}-x, y, z$.

5. Comparison with the $NiAl_2O_4$–Ni_2SiO_4 system

The previous studies of the $NiAl_2O_4$–Ni_2SiO_4 system (Ma, 1974; Akaogi *et al.*, 1982) indicated pressure as being the main factor controlling the relative stabilities of the spinelloid phases. For instance, phases III, IV and V were reported to form at increasingly high pressures in agreement with minor density increases (for identical compositions) and with a reduction in the amount of tetrahedral corner sharing in their crystal structures. But no clear correlation was established between the formation of spinelloid phases and the other variables, such as temperature and chemical composition.

By contrast, our study of the $NiGa_2O_4$–Ni_2SiO_4 system has been carried out at constant pressure (1 atm) and it clearly establishes a link between the spinelloid structure types and their chemical compositions. As described in the previous section, this link is achieved by means of a close correlation

Table 9. *Bond lengths* (Å) *and angles* (°) *in phase* II

M(2)—O(1*A*)	2.047 (3)	*M*(3)—O(1*B*)	2.063 (3)	*M*(4)—O(3)	2.047 (4)
M(2)—O(1*B*)	2.047 (3)	*M*(3)—O(1*D*)	2.063 (3)	*M*(4)—O(4)	2.069 (4)
M(2)—O(1*D*)	2.047 (3)	*M*(3)—O(2*A*)	2.042 (4)	*M*(4)—O(5)	2.051 (3)
M(2)—O(1*E*)	2.047 (3)	*M*(3)—O(2*D*)	2.042 (4)	*M*(4)—O(1*C*)	2.051 (4)
M(2)—O(4*A*)	2.073 (4)	*M*(3)—O(5*A*)	2.045 (4)	*M*(4)—O(4*C*)	2.069 (4)
M(2)—O(4*B*)	2.073 (4)	*M*(3)—O(5*D*)	2.045 (4)	*M*(4)—O(5*G*)	2.051 (3)
M(1)—O(2)	2.019 (4)	*T*(2)—O(2*C*)	1.809 (5)	*T*(3)—O(3)	1.703 (5)
M(1)—O(5)	2.003 (3)	*T*(2)—O(3*A*)	1.833 (5)	*T*(3)—O(3*A*)	1.703 (5)
M(1)—O(2*B*)	2.019 (4)	*T*(2)—O(5*C*)	1.806 (4)	*T*(3)—O(4*B*)	1.711 (6)
M(1)—O(5*B*)	2.003 (3)	*T*(2)—O(5*F*)	1.806 (4)	*T*(3)—O(4*D*)	1.711 (6)
M(1)—O(5*E*)	2.003 (3)				
M(1)—O(5*G*)	2.003 (3)				

O(1*A*)—*M*(2)—O(1*D*)	89.5 (2) × 2	O(1*B*)—*M*(3)—O(1*D*)	89.6 (2)
O(1*B*)—*M*(2)—O(1*D*)	90.5 (2) × 2	O(1*B*)—*M*(3)—O(2*A*)	90.5 (1) × 2
O(1*A*)—*M*(2)—O(4*A*)	95.2 (2) × 2	O(2*A*)—*M*(3)—O(2*D*)	89.8 (2)
O(1*B*)—*M*(2)—O(4*A*)	84.8 (2) × 4	O(1*B*)—*M*(3)—O(5*A*)	84.8 (1) × 2
		O(1*D*)—*M*(3)—O(5*A*)	97.4 (1) × 2
O(3)—*M*(4)—O(4)	93.7 (2) × 2	O(2*A*)—*M*(3)—O(5*A*)	86.7 (2) × 2
O(3)—*M*(4)—O(5)	96.5 (1) × 2	O(2*D*)—*M*(3)—O(5*A*)	91.0 (2) × 2
O(4)—*M*(4)—O(5)	92.0 (1) × 2		
O(4)—*M*(4)—O(1*C*)	84.8 (2) × 2	O(2)—*M*(1)—O(5)	91.5 (1) × 4
O(5)—*M*(4)—O(1*C*)	85.0 (1) × 2	O(5)—*M*(1)—O(2*B*)	88.5 (1) × 4
O(4)—*M*(4)—O(4*C*)	89.0 (2)	O(5)—*M*(1)—O(5*G*)	87.9 (2) × 2
O(5)—*M*(4)—O(5*G*)	85.3 (2)	O(5)—*M*(1)—O(5*E*)	92.1 (2) × 2
O(2*C*)—*T*(2)—O(3*A*)	113.4 (2)	O(3)—*T*(3)—O(3*A*)	112.9 (3)
O(2*C*)—*T*(2)—O(5*C*)	111.6 (1) × 2	O(3)—*T*(3)—O(4*B*)	107.6 (1) × 4
O(3*A*)—*T*(2)—O(5*C*)	104.2 (1) × 2	O(4*B*)—*T*(3)—O(4*D*)	113.6 (3)
O(5*C*)—*T*(2)—O(5*F*)	111.4 (2)		

Symmetry codes: *A*, $x, y, z+1$; *B*, $-x, -y, -z$; *C*, $\frac{1}{2}-x, \frac{1}{2}-y, \frac{1}{2}-z$; *D*, $\frac{1}{2}-x, y, \frac{1}{2}-z$; *E*, $x, -y, -z$; *F*, $\frac{1}{2}+x, \frac{1}{2}-y, \frac{1}{2}-z$; *G*, $-x, y, z$.

between the occupancies of the tetrahedral sites and their topological configurations (defined in terms of corner-sharing with adjacent tetrahedra). On the one hand, the spinel structure with isolated tetrahedra of fixed regular geometry only accommodates a limited amount of silicon (6 mol% Ni_2SiO_4), probably because of the large difference between the Ga—O (1.85 Å) and Si—O (1.64 Å) tetrahedral bonds. On the other hand, the lower symmetry and the introduction of more and more *T* boundaries in the structures of phases V, I and II allow a greater distortion and a size reduction of the tetrahedral sites, which are required to accommodate larger amounts of silicon (27–38 mol% Ni_2SiO_4). The opposite is also true: larger Si contents are needed to satisfy the bonding requirements of the three-coordinated O atoms generated at the *T* boundaries and corresponding to corners shared between adjacent tetrahedra.

Although it was not the purpose of the present work to investigate the phase diagram of the $NiGa_2O_4$–Ni_2SiO_4 system in detail, it nevertheless reveals both similarities and differences with the spinelloid phase relations of the $NiAl_2O_4$–Ni_2SiO_4 system (Ma, 1974; Akaogi *et al.*, 1982). Firstly, phase I is found to exist in both systems at atmospheric pressure and with a similar composition. The aluminosilicate phase has been reported to exist over a relatively wide composition range (9 mol% Ni_2SiO_4; see Ma, 1974), as a result of the easy Al/Si substitution combined with the effects of high temperature and high pressure. The composition range for the gallosilicate phase would probably be comparatively narrower due to the larger size difference between Ga and Si atoms. This effect is indeed observed for the atmospheric pressure spinel solid solution, which is limited to about 6 mol% Ni_2SiO_4 in the gallosilicate system but extends up to about 12 mol% Ni_2SiO_4 at 1873 K in the aluminosilicate system (Ma, 1974). Secondly, although phase II had originally been reported to form only at moderately high pressure in the $NiAl_2O_4$–Ni_2SiO_4 system (Ma, 1974), later studies showed that it could also form at 1 atm with a composition close to 40 mol% Ni_2SiO_4 (Akaogi & Navrotsky, 1984), which is similar to that found in the present work for the phase II of the $NiGa_2O_4$–Ni_2SiO_4 system. This similarity between phases I and II of the two systems extends further to the details of their atomic distributions: the Al/Si distribution in the aluminosilicate phases could not be directly determined by X-ray diffraction (Ma, Sahl & Tillmanns, 1975; Ma & Tillmanns, 1975) but the analysis of bond-length data and bond valences indicates that the tetrahedral Si contents increase in the same order, $T(1) < T(2) < T(3)$, as found for the gallosilicate phases. This result supports the suggestion that the driving force behind the partial tetrahedral (and octahedral) ordering observed in the spinelloid structures is the necessity to achieve local charge balance, in particular at the *T* boundaries.

A major difference between the $NiGa_2O_4$–Ni_2SiO_4 and $NiAl_2O_4$–Ni_2SiO_4 systems concerns the stability field of phase V, which readily forms at 1 atm in the former system but has only been observed in products quenched from above 7 GPa in the latter system (Akaogi *et al.*, 1982). Furthermore, the composition of the aluminosilicate phase has been reported to be around 50 mol% Ni_2SiO_4, whereas that of the gallosilicate phase is much less Si rich: approximately 27 mol% Ni_2SiO_4 at 1 atm pressure. As mentioned previously, such a shift in chemical composition may be partly and qualitatively accounted for by the effect of high pressure: the longer and weaker Al(Ga)—O bonds are expected to be more compressible than the Si—O bond and, consequently, greater Al(Ga)/Si mixing should be possible at high pressures while retaining similar oxygen packings in the individual spinelloid structures. In that respect, it is noteworthy that the composition of the phase V recently synthesized at 7 GPa in the Fe_3O_4–Fe_2SiO_4 system is indeed richer in silicon (32 mol% Fe_2SiO_4; see Ross *et al.*, 1992) than the atmospheric pressure phase V of the $NiGa_2O_4$–Ni_2SiO_4 system, in spite of similar Fe^{III}—O and Ga—O tetrahedral bond lengths (1.87 and 1.85 Å, respectively; see Shannon,

Table 10. *Correlation between structure type, tetrahedral populations and chemical compositions for the nickel gallosilicate spinelloids*

	% Si			No. of *T* sites	Composition	Structural
	T(1)	*T*(2)	*T*(3)	in cell	(mol% Ni_2SiO_4)	sequence*
Spinel	6	–	–	4*T*(1)	6.0	S^2
Phase V	12	35	–	2*T*(1) + 4*T*(2)	27.3	TS^2
Phase IV				4*T*(1) + 16*T*(2)	28†	$(TS^2TS)^2$
Phase III				8*T*(2)	32†	$(TS)^2$
Phase I	10	28	65	2*T*(1) + 4*T*(2) + 2*T*(3)	32.7	T^2S^2
Phase II	–	24	66	8*T*(2) + 4*T*(3)	38.0	$(T^2S)^2$

* After Hyde *et al.* (1982).

† Hypothetical compositions based on the average tetrahedral populations of phases V and I.

1976). Following this line of reasoning, a nickel aluminosilicate phase V synthesized at low pressure could be expected to have a more Al- or $NiAl_2O_4$-rich composition, closer to that of the gallosilicate phase. This then leads to the question as to why phase V does not form at room pressure in the $NiAl_2O_4$–Ni_2SiO_4 system, whereas phases I and II are readily obtained. The answer to that question may be linked to the formation of a more extensive spinel solid solution in that system (see above), which could result in a greater stabilization of a mixture of spinel plus phase I relative to a single phase V of intermediate composition. A similar situation occurs in the $MgGa_2O_4$–Mg_2GeO_2 system in which the only spinelloid phases forming at atmospheric pressure are phase III at around 50 mol% Mg_2GeO_4 and a wide-spinel solid solution up to about 30 mol% Mg_2GeO_4 (Barbier & Hyde, 1986; Leinenweber & Navrotsky, 1989).

A further difference between the nickel gallosilicate and aluminosilicate systems corresponds to the absence in the former of the spinelloid phases III and IV, even as minor amounts in microscopic intergrowths examined by transmission electron microscopy. These two phases are structural intermediates between phases I and V (see, for example, Hyde *et al.*, 1982) and, according to the structure/composition relationship described earlier, they might have been expected to form at 1 atm with compositions of approximately 32 and 28 mol% Ni_2SiO_4, intermediate between those of phases I and V (see Table 10). However, it appears that the formation of the latter phases is favoured over this narrow composition interval of only a few mol% Ni_2SiO_4 (between 27 mol% for phase V and 33 mol% for phase I) and their stabilization may be due, in part, to the fact that their structures allow better silicon partitioning: for instance, the number of crystallographically distinct tetrahedral sites available per tetrahedral atom in the individual spinelloid unit cells is equal to 2/6 and 3/8 for phases V and I as compared to only 2/20 and 1/8 for phases IV and III (see Table 10). Thus, through partial atomic ordering, the structures of phases V and I may be able to absorb more easily the strain associated with the size mismatch between the Ga and Si tetrahedral atoms. This idea would then imply that the minimization of strain energy may be a significant factor for the stabilization of the spinelloid phases, thus counteracting the configurational entropy effect associated with cation mixing (Akaogi & Navrotsky, 1984; Leinenweber & Navrotsky, 1989).

Overall, the prediction and explanation of the relative stabilities of individual spinelloid phases (see, for example, Price & Yeomans, 1984; Price *et al.*, 1985) in pseudobinary systems, such as $NiAl_2O_4$–Ni_2SiO_4, $NiGa_2O_4$–Ni_2SiO_4, $MgGa_2O_4$–Mg_2GeO_4, $MgFe_2O_4$–Mg_2GeO_4 or Fe_3O_4–Fe_2SiO_4, must involve a complex combination of compositional, structural and thermodynamic effects. Besides their dependence on the pressure and temperature variables, the spinelloid phase relations in these various systems clearly also depend, in a subtle way, on the nature of the atomic species involved. Further understanding of their crystal chemistry would require the systematic investigation of the spinelloid crystal structures (in particular, their atomic distributions) as a function of temperature and pressure.

This work was supported by a research grant to JB from the Natural Sciences and Engineering Research Council of Canada. The help of Dr J. Britten with the data collection is also acknowledged. The authors are thankful to A. Navrotsky for a helpful review.

References

Akaogi, M., Akimoto, S., Horioka, K., Takahashi, K. & Horiuchi, H. (1982). *J. Solid State Chem.* **44**, 257–267.

Akaogi, M. & Navrotsky, A. (1984). *Phys. Chem. Miner.* **10**, 166–172.

Akimoto, S. & Sato, Y. (1968). *Phys. Earth Planet. Inter.* **1**, 498–505.

Barbier, J. (1989). *Eur. J. Mineral.* **1**, 39–46.

Barbier, J. & Hyde, B. G. (1986). *Phys. Chem. Miner.* **13**, 382–392.

Brown, I. D. & Altermatt, D. (1985). *Acta Cryst.* **B41**, 244–247.

Guyot, F., Gwanmesia, M. & Liebermann, R. C. (1991). *Geophys. Res. Lett.* **18**, 89–92.

Hammond, R. & Barbier, J. (1991). *Phys. Chem. Miner.* **18**, 184–190.

Horioka, K., Nishiguchi, M., Morimoto, N., Horiuchi, H., Akaogi, M. & Akimoto, S. (1981). *Acta Cryst.* **B37**, 635–637.

Horioka, K., Takahashi, K., Morimoto, N., Horiuchi, H., Akaogi, M. & Akimoto, S. (1981). *Acta Cryst.* **B37**, 638–640.

Horiuchi, H., Akaogi, M. & Sawamoto, S. (1982). In *High Pressure Research in Geophysics*, edited by S. Akimoto & M. H. Manghnani. Boston: Reidel.

Horiuchi, H., Horioka, K. & Morimoto, N. (1980). *J. Mineral. Soc. Jpn Spec. Issue*, **2**, 253–264.

HYDE, B. G., WHITE, T. J., O'KEEFFE, M. & JOHNSON, A. W. S. (1982). *Z. Kristallogr.* **160**, 53–62.
LEINENWEBER, K. & NAVROTSKY, A. (1989). *Phys. Chem. Miner.* **16**, 497–502.
MA, C. B. (1974). *Contrib. Mineral. Petrol.* **45**, 257–279.
MA, C. B & SAHL, K. (1975). *Acta Cryst.* B**31**, 2141–2143.
MA, C. B., SAHL, K. & TILLMANNS, E. (1975). *Acta Cryst.* B**31**, 2137–2139.
MA, C. B. & TILLMANNS, E. (1975). *Acta Cryst.* B**31**, 2139–2141.
MADON, M. & POIRIER, J. P. (1983). *Phys. Earth Planet. Inter.* **33**, 31–44.
MORIMOTO, N., AKIMOTO, S., KOTO, K. & TOKONAMI, M. (1969). *Science*, **165**, 586–588.
MORIMOTO, N., TOKONAMI, M., KOTO, K. & NAKAJIMA, S. (1972). *Am. Mineral.* **57**, 62–75.
MORIMOTO, N., TOKONAMI, M., WATANABE, M. & KOTO, K. (1974). *Am. Mineral.* **59**, 475–485.
PRICE, G. D. (1983). *Phys. Chem. Miner.* **10**, 77–83.
PRICE, G. D., PARKER, S. C. & YEOMANS, J. (1985). *Acta Cryst.* B**41**, 231–239.
PRICE, G. D., PUTNIS, A., AGRELL, S. O. & SMITH, D. G. W. (1983). *Can. Mineral.* **21**, 29–35.
PRICE, G. D. & YEOMANS, J. (1984). *Acta Cryst.* B**40**, 448–454.
RINGWOOD, A. E. & MAJOR, A. (1970). *Phys. Earth Planet. Inter.* **3**, 89–108.
ROSS, C. R., ARMBRUSTER, T. & CANIL, D. (1992). *Am. Mineral.* **77**, 507–511.
SAWAMOTO, S. & HORIUCHI, H. (1990). *Phys. Chem. Miner.* **17**, 293–300.
SHANNON, R. D. (1976). *Acta Cryst.* A**32**, 751–767.
SHELDRICK, G. M. (1990). *SHELXTL-Plus.* Release 4.1 for Siemens *R3m/V* crystallographic system. Siemens Crystallographic Research Systems, New Jersey, USA.
SKOWRON, A. & BROWN, I. D. (1990). *Acta Cryst.* C**46**, 527–531.
SYONO, Y., AKIMOTO, S. & MATSUI, Y. (1971). *J. Solid State Chem.* **3**, 369–380.

Acta Cryst. (1993). B**49**, 213–216

The Geometry of Twinning in $HoCu_2$

BY JOHN R. SEIDENSTICKER AND EARLE R. RYBA

Department of Materials Science and Engineering, The Pennsylvania State University, University Park, PA 16802, *USA*

(*Received* 16 *October* 1991; *accepted* 2 *September* 1992)

Abstract

The twinning relationship in the intermetallic compound $HoCu_2$ was determined by single-crystal X-ray diffraction techniques. A 60° rotation about the *b* axis between the two components of the twins was found. The twin plane is (103). The measured single-crystal lattice parameters deviate from those obtained from powder data by 0.03 Å for *a* and 0.10 Å for *c*. These deviations may be due to strain in the structure caused by the twinning. The same twinning geometry is believed to hold true for the other rare-earth–metal ($RE M_2$) intermetallic compounds with the KHg_2-type structure that exhibit massive twinning. This twinning may be the result of a high-temperature martensitic-type phase transformation.

Introduction

The microstructures of rare-earth–metal ($RE M_2$; *M* = Cu, Zn) intermetallic compounds exhibit extensive twinning (Kejriwal, 1962; Chiotti, Mason & Gill, 1963; Chiotti & Mason, 1965, 1967; Mason & Chiotti, 1968; Michel & Ryba, 1969), the origin of which is thought to be a high-temperature martensitic-type transformation (Chiotti, Mason & Gill, 1963; Mason & Chiotti, 1968). In this paper, the results of a study are presented in which the twinning relationship in $HoCu_2$ was determined through the use of single-crystal X-ray diffraction techniques.

Most of the $RE M_2$ compounds, including $HoCu_2$, exhibit the orthorhombic KHg_2- or $CeCu_2$-type structure (Duwell & Baenziger, 1955; Larson & Cromer, 1961). Storm & Benson (1963) determined the lattice parameters for $HoCu_2$ to be $a = 4.280\ (5)$, $b = 6.759\ (5)$ and $c = 7.290\ (5)$ Å, while Smetana, Sima & Lebech (1986) determined the atom positions (space group *Imma*) to be Ho: 4(*e*) [$z = 0.544\ (1)$] and Cu: 8(*h*) [$y = 0.056\ (1)$, $z = 0.162\ (1)$]. The structure, using these lattice and positional parameters, is shown in Fig. 1.

Experimental

A sample was prepared by sealing stoichiometric amounts of 99.5% Ho and 99.999% Cu in a tantalum crucible. The mixture was then melted, slowly cooled and finally annealed to homogenize the alloy. Crystal fragments chosen from this sample were coated with a polymer resin to suppress oxidation. A powder sample was prepared by crushing a portion of the alloy and passing the powder through a 325 mesh sieve; the powder pattern was run immediately after preparation of the sample. A step scan (0.02° step size, 4 s counting time) was performed over the range 15–120° 2θ on a Scintag powder diffractom-

0108-7681/93/020213-04$06.00